Excited State Properties of Lanthanide(III) Complexes with a Nonadentate Bispidine Ligand

Laura Abad-galán, Patrick Cieslik, Peter Comba, Michael Gast, Olivier Maury, Lucca Neupert, Amandine Roux, Hubert Wadepohl

Chemistry
A European
Journal

Chemistry
Europe
European Chemical
Societies Publishing

Reprint

WILEY-VCH

Excited State Properties of Lanthanide(III) Complexes with a Nonadentate Bispidine Ligand

Laura Abad-Galán,[a] Patrick Cieslik+,[b] Peter Comba,*[b, d] Michael Gast,[b] Olivier Maury,*[a] Lucca Neupert,[b] Amandine Roux,[a] and Hubert Wadepohl[b]

Dedicated to Professor Wolfgang Kaim on the occasion of his 70th birthday.

Abstract: Eu^{III}, Tb^{III}, Gd^{III} and Yb^{III} complexes of the nonadentate bispidine derivative L^2 (bispidine = 3,7-diazabicyclo [3.3.1]nonane) were successfully synthesized and their emission properties studied. The X-ray crystallography reveals full encapsulation by the nonadentate ligand L^2 that enforces to all Ln^{III} cations a common highly symmetrical capped square antiprismatic (CSAPR) coordination geometry (pseudo C_{4v} symmetry). The well-resolved identical emission spectra in solid state and in solution confirm equal structures in both media. As therefore expected, this results in long-lived excited states and high emission quantum yields ($[Eu^{III}L^2]^+$, H_2O, 298 K, $\tau = 1.51$ ms, $\phi = 0.35$; $[Tb^{III}L^2]^+$, H_2O, 298 K, $\tau = 1.95$ ms, $\phi = 0.68$). Together with the very high kinetic and thermodynamic stabilities, these complexes are a possible basis for interesting biological probes.

Introduction

Luminescent lanthanide complexes generally have very narrow and metal-ion-specific emission spectra, large pseudo-Stokes shifts, relatively high quantum yields ϕ (for Eu^{III} and Tb^{III}, *e.g.*, ϕ around 20–30%[1,2] and 60%[3] is common, and values up 90%[4–6] have been reported), and long emission lifetimes of the order of milliseconds.[7,8] Potential applications include emissive optical materials and various kinds of biological probes, also including in-cell imaging.[9–15] Major challenges for lanthanide-based luminescence probes are the quantum yield and lifetime optimization,[12,16] and consequently, the limitation of non-radiative deactivation processes like vibrational and/or rotational quenching or back-energy transfer.[17–19] Quenching by the O–H overtones of water often occurs from coordinated H_2O[20,21] but may also be due to H_2O in the second coordination sphere,[22] and therefore, full encapsulation of the metal ions by the ligand is of great importance. Typical ligands used in the area are octa- and nonadentate macrocyclic[16,23–30] and cryptate based ligands[5,8,31,32] as well as the tetradentate HOPO family[25,33–36] and a ditopic ligand producing helicates,[37–39] as shown in Scheme 1, together with the published octadentate bispidine ligand L^1[40,41] and its nonadentate derivative L^2 discussed here. Ln^{III} ions often realize coordination numbers of 8 or 9.[34,35,42–44] In particular, the bispidine-Ln^{III} complexes reported so far were all 9-coordinate with the octadentate L^1 and a monodentate co-ligand, H_2O, in aqueous solution.[40,41,45] For CN = 9, the coordination geometries most commonly observed are trigonal capped prismatic (TCTPR)[46–48] or spherical capped square antiprismatic (CSAPR)[41,49] (see Figure 1), the latter generally leading to more intense 4f–4f electronic transitions due to the odd-parity asymmetry of the structure.[49] Therefore, ligands that enforce highly symmetrical CSAPR geometries are of particular interest.

The rigidity of the bispidine platform[50–52] and the versatility in terms of denticity and donor types as well as the synthetic

Figure 1. Graphical illustration of a tricapped trigonal prismatic (left), spherical capped square antiprismatic (middle) and muffin (right) coordination of Ln^{III} ions.

[a] Dr. L. Abad-Galán, Dr. O. Maury, Dr. A. Roux
Université de Lyon, ENS de Lyon, Laboratoire de Chimie, CNRS UMR 5182
Université Claude Bernard Lyon 1
69342 Lyon (France)
E-mail: olivier.maury@ens-lyon.fr

[b] Dr. P. Cieslik,+ Prof. Dr. P. Comba, Dr. M. Gast, L. Neupert, Prof. Dr. H. Wadepohl
Universität Heidelberg
Anorganisch-Chemisches Institut, INF 270
69120 Heidelberg (Germany)
E-mail: peter.comba@aci.uni-heidelberg.de

[d] Prof. Dr. P. Comba
Universität Heidelberg
Interdisciplinary Center for Scientific Computing
69120 Heidelberg (Germany)

[+] This work is part of the PhD thesis of Dr. Patrick Cieslik.

Supporting information for this article is available on the WWW under https://doi.org/10.1002/chem.202005459

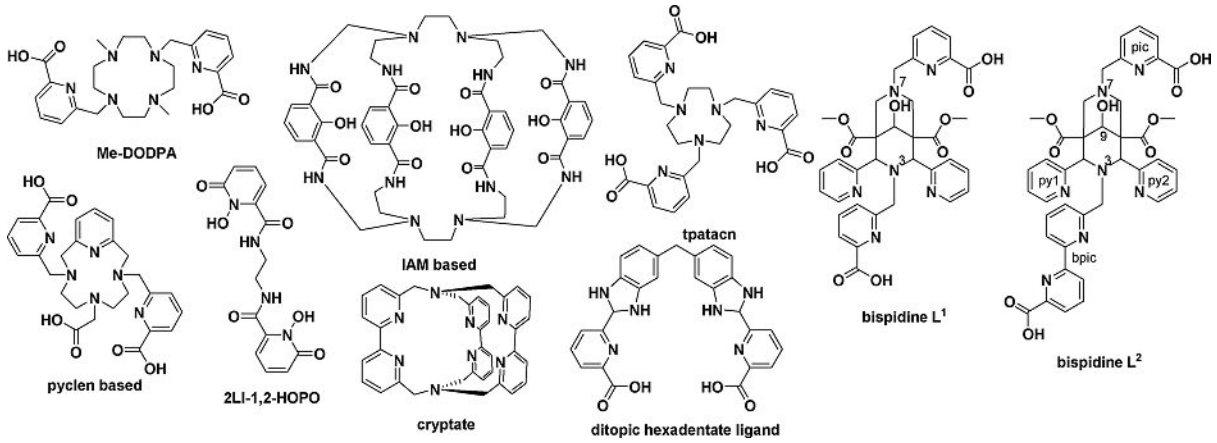

Scheme 1. Typical structures of commonly used ligands for Ln^{III} complexation, and of the bispidine derivatives L^1 and L^2 with the numbering of bispidine L^2.

availability of a large number of ligands, makes this type of chelator a favorable platform for a variety of applications, including Ln^{III} based luminescence probes.[53–56] Moreover, with negatively charged donors (*e.g.* carboxylates) or non-coordinating substituents, the overall charge of the complexes may be affected, allowing to tune the cell permeability for in-cell imaging. Also, a number of bispidine derivatives have been reported that allow their attachment to biological vectors; of particular interest is the substitution at C9, *i.e.* remote from the coordination site.[57–60]

We have recently reported nonacoordinate Ln^{III} complexes with the octadentate bispidine L^1 (Scheme 1) with CSAPR coordination geometries, which, although coordination of a water molecule was detected in the first coordination sphere, lead to Ln^{III} complexes with extended luminescent lifetimes and appreciable quantum yields.[41] Importantly, these Ln^{III} complexes have large complex stabilities and also show exceedingly high kinetic stabilities, as usually observed with bispidine metal complexes.[40,61,62] To further improve the system, the analogous nonadentate ligand L^2 with the same rigid ligand scaffold and predictably similar coordination geometry was believed to significantly enhance the luminescence lifetime and provide higher quantum yields by suppressing the detrimental water coordination. Therefore, we now report the synthesis of the nonadentate bispidine L^2 and its Ln^{III} complexes and discuss here their photophysical properties.

Ligand Synthesis

The synthesis of the nonadentate ligand L^2 was achieved by using two different protecting groups at the bispidine amine donors N^3 and N^7. The synthesis starts by building up the bispidone scaffold (1) in two consecutive double Mannich reactions (Scheme 2). The literature-known piperidone P[63] was synthesized with commercially available starting materials, and this allows to prepare it on a large scale (currently up to 100 g batches). The piperidone was reacted with formaldehyde and 2,4-dimethoxybenzylamine to obtain the double amine-protected bispidone 1. To prevent ring opening from retro-Mannich reaction, the keto group at C9 of was reduced with sodium borohydride, yielding bispidol 2. Deprotection with trifluoroacetic acid led to intermediate 3 with one free amine, suitable for coupling through nucleophilic substitution to *tert*-butyl 6-(bromomethyl)picolinate 7.[40] The benzylated bispidine 4 was hydrogenated with palladium on activated charcoal to yield the secondary amine precursor 5.[64] *tert*-butyl 6′-(bromomethyl)-[2,2′-bipyridine]-6-carboxylate 8 was obtained from 6′-methyl-[2,2′-bipyridine]-6-carboxylic acid 9[65] by applying a known procedure to compound 7 (Scheme 3). Alkylation was carried out as before for the synthesis of 4. The *tert*-butyl ester groups of precursor 6 were finally removed by treatment with TFA to obtain ligand L^2 in an overall yield of 5%. All bispidine derivatives were obtained by purification via crystallization, and the synthetic steps were carried out in multigram scales (see Experimental Section for details).

Metal complexes

Equimolar solutions of the metal salts and ligand L^2 in methanol/water (1:1) were combined and diethylether diffusion afforded $[LnL^2][NO_3]$ (for Ln = Tb, Gd and Yb), and $[Eu\ L^2][CF_3CO_2]$ complexes with 40–70% yield (Scheme 4). The formation of the metal complexes was confirmed by HRMS, elemental analyses and photophysical measurements. Crystals of all four Ln^{III} complexes, suitable for single-crystal X-ray analyses, were obtained by diffusion of diethylether into the methanolic solution of the complexes (Figure 1). However, the counter ion of $[EuL^2][CF_3CO_2]$ could not be refined.[66] The geometry of the cation could, however, be established and refined satisfactorily. Therefore, only the salient geometric features are discussed and presented in Table 1.[66] As seen in Figure 2, in all structures the central Ln^{III} ions are coordinated to all nine donor atoms (N_7O_2) of the doubly deprotonated ligand, fully saturating the coordination sphere and therefore avoiding the detrimental coordination of water molecules. Selected bond lengths and angles are compared in Table 1. It emerges that, in

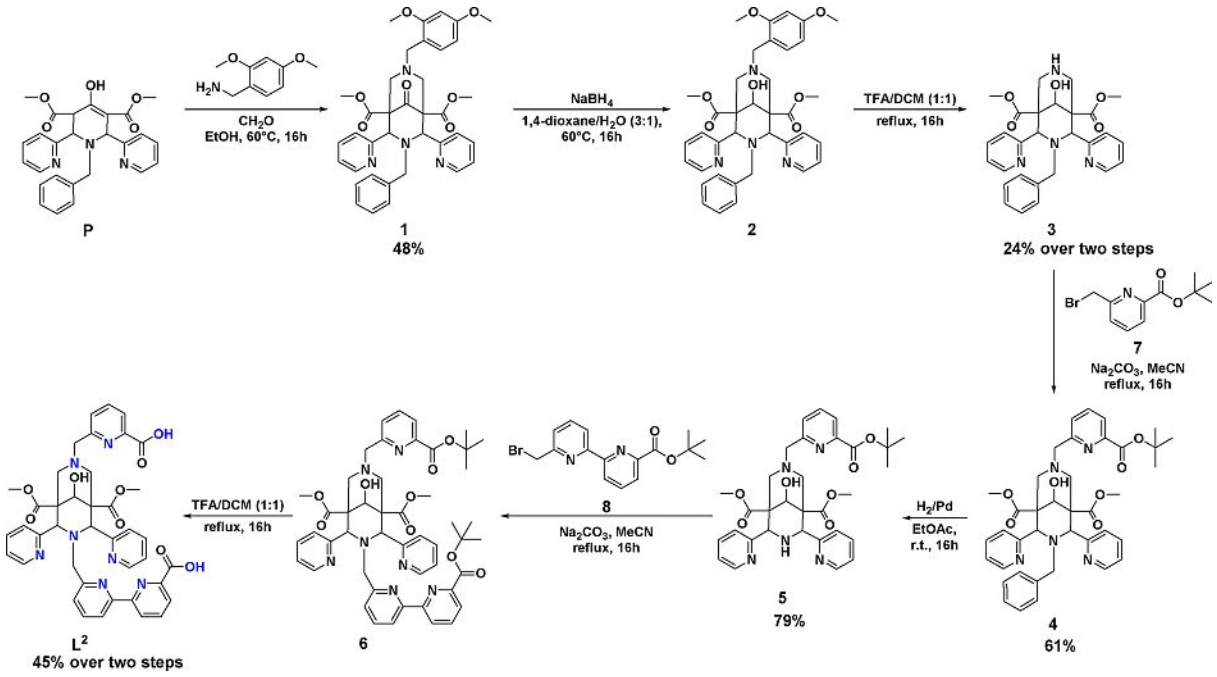

Scheme 2. Synthetic route to the nonadentate bispidine derivative L^2. Coordinating atoms of the ligand are colored in blue.

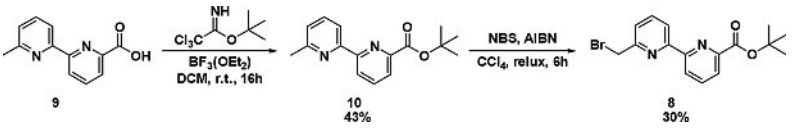

Scheme 3. Synthesis of tert-butyl 6′-(bromomethyl)-[2,2′-bipyridine]-6-carboxylate (8).

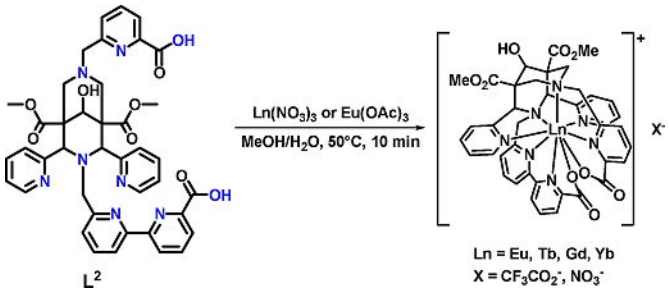

Scheme 4. Synthesis of the $[LnL^2][X]$ complexes ($X = CF_3CO_2^-$ for Eu, $X = NO_3^-$ for Tb, Gd and Yb).

agreement with the lanthanide contraction, metal-donor bond lengths are decreasing with increasing atomic number. This is especially obvious for the M-Nbpic1 and M–N7 bonds, where the distances decrease by $\Delta_{Eu\text{-}Yb} = 0.12$ Å and 0.09 Å, respectively. The metal-oxygen bond lengths show similar trends (M-Opic: $\Delta_{Eu\text{-}Yb} = 0.10$ Å; M-Obpic: $\Delta_{Eu\text{-}Yb} = 0.09$ Å). The rigidity of the backbone is supported by the constant N3···N7 distances of around 3.00 Å. An overlay plot of all structures of the $[LnL^2]^+$ complex cations well visualizes the rigidity of the ligand due to the bispidine platform (Figure 3).

Continuous shape analyses using the program SHAPE 2.1[67] were carried out to investigate the coordination geometry (see Supporting Information, Table S2). The smallest continuous shape measure values (CShM) are also presented in Table 1 ($0 <$ CShM < 100, CShM $= 0$ indicates the perfect polyhedron). According to the experimentally determined CShM values, the coordination geometry of all $[LnL^2][X]$ complexes can be considered as a slightly distorted spherically capped square antiprismatic (CSAPR-9, C_{4v}), with the Muffin (MFF-9, C_s) slightly less well matching. A representation of the coordination polyhedra is shown in Figure 4. For the CSAPR geometry, the two square planes with internal torsional angles between 5.0° and 12.2° are rotated by 15–30° to each other. The distances of the centroids of the two square planes are 2.6 Å on average (Table 2). The centroid-N3 distances only differ slightly and are in all cases close to 1.6 Å. The centroid-centroid-N3 angles are close to 180°, and the dihedral angles are close to 0°, in excellent agreement with the shape analysis (see Supporting Information for a detailed discussion of the crystal structures).

Table 1. Selected bond lengths [Å] and angles [°] in the crystal structures of $[LnL^2][X]$ complexes (Ln = Eu,[a] Gd, Tb, Yb; X = CF_3CO_2, NO_3) together with selected CShM values.

	$[EuL^2][CF_3CO_2]$[a]	$[GdL^2][NO_3]$	$[TbL^2][NO_3]$·solv	$[YbL^2][NO_3]$
M–N3	2.665(5)	2.650(3)	2.652(2)	2.619(6)
M–N7	2.640(5)	2.622(3)	2.598(2)	2.553(6)
M–Npy1	2.580(5)	2.616(3)	2.693(3)	2.549(6)
M–Npy2	2.676(5)	2.692(3)	2.597(3)	2.664(7)
M–Npic	2.512(5)	2.520(3)	2.491(2)	2.438(6)
M–Nbpic1	2.549(5)	2.525(3)	2.504(10)[b] 2.459(13)[b]	2.434(6)
M–Nbpic2	2.520(5)	2.502(3)	2.492(14)[b] 2.494(18)[b]	2.444(6)
M–Opic	2.379(4)	2.378(2)	2.338(2)	2.284(5)
M–Obpic	2.364(4)	2.335(2)	2.358(19)[b] 2.28(2)[b]	2.278(5)
N3···N7	3.007(5)	3.017(3)	2.996(3)	2.983(5)
Npy1···Npy2	4.721(5)	4.734(3)	4.704(4)	4.651(5)
N3–M–N7	69.06(14)	69.81(9)	69.58(7)	70.41(18)
Npic–M–Obpic	70.13(16)	72.42(9)	72.8(11)[b] 71.6(15)[b]	71.4(2)
Npy1–M–Npy2	127.83(16)	126.20(9)	125.56(8)	126.24(19)
Npic-Obpic-Nbpic2-Opic	11.43	10.81	8.29[b] 7.50[b]	5.02
Opic-Npic-Obpic-Nbpic2	12.18	11.55	8.94[b] 7.52[b]	5.10
Npy2-N7-Npy1-Nbpic1	6.36	8.75	8.40[b] 10.92[b]	10.16
Npy1-N7-Npy2-Nbpic1	5.46	7.70	9.52[b] 10.28[b]	9.80
CShM (CSAPR-9, C_{4v})	1.682	1.615	1.748	1.380
CShM (MFF-9, C_s)	2.051	1.995	2.093	1.828

[a][66]; [b] 0.57:0.43 disorder.

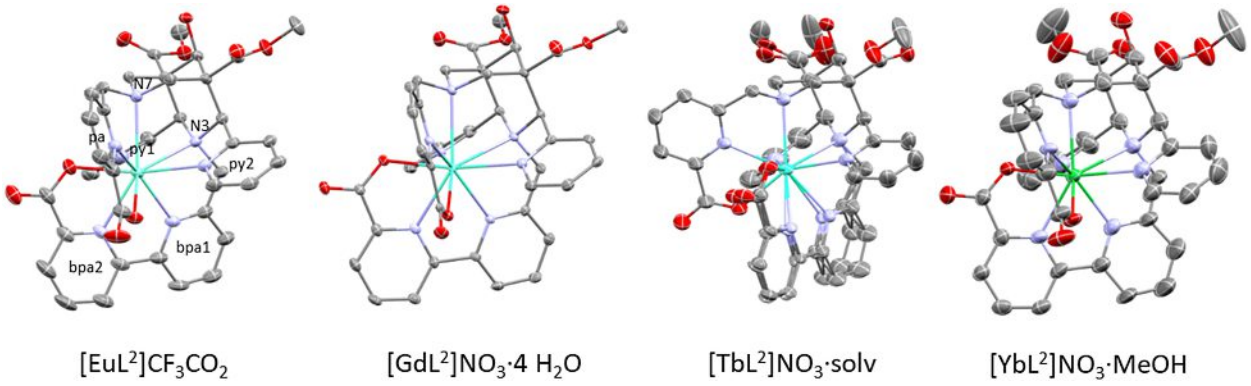

Figure 2. ORTEP plots of the $[LnL^2]^+$ complex cations. Atoms are shown at 50% probability; hydrogen atoms, solvent molecules and anions are omitted for clarity.[66]

Table 2. Distances [Å] and angles [°] in the coordination polyhedron of $[LnL^2]^+$ complex cations.

	$[EuL^2][CF_3CO_2]$[a]	$[GdL^2][NO_3]$	$[TbL^2][NO_3]$[b]	$[YbL^2][NO_3]$
X_1-X_2[c]	2.597	2.570	2.543 2.585	2.477
X_2-N3[c]	1.600	1.590	1.590 1.590	1.606
X_1-X_2-N3[c]	173.03	173.22	174.93 173.19	175.79
θ[d]	0.96	1.83	0.81 2.13	1.06

[a][66]; [b] 0.57:0.43 disorder; [c] centroid of the square planes: X_1 = Npy1-N7-Npy2-Nbpic1, X_2 = Npic-Obpic-Nbpic2-Opic; [d] dihedral angles between the mean plane of the two square planes.

Photophysical Investigation

For the photophysical characterization, absorption, excitation, and emission spectra as well as emission quantum yields and excited state lifetimes of all complexes, where possible and useful, were measured in the solid state (amorphous phase) and in diluted aqueous solution. The main data are summarized in Table 3.

The absorption profiles of all complexes in water are identical and show the characteristic π–π* transitions of the pyridine and picolyl moieties at 260–280 nm,[41] as well as a red shifted π–π* band at ~315 nm, attributed to the bipyridine arm

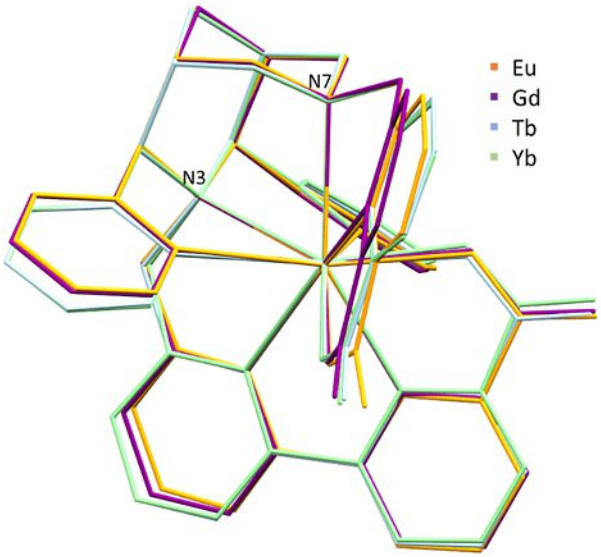

Figure 3. Overlay of crystal structures of $[LnL^2]^+$ complex cations (orange: Eu, purple: Gd, blue: Tb, green: Yb). Hydrogen atoms, solvent molecules, anions and non-coordinating residues have been omitted for clarity.[66]

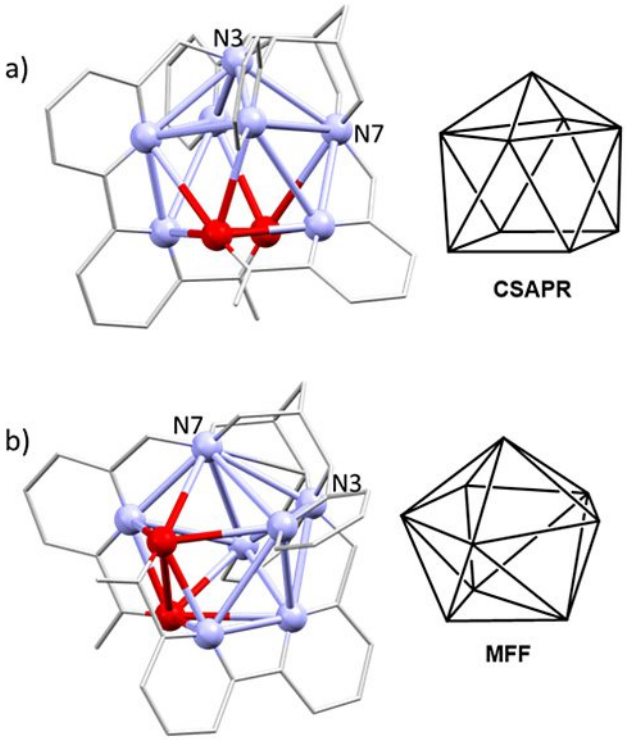

Figure 4. Depiction of the coordination polyhedra CSAPR (a) and muffin (b), derived from the $[YbL^2]^+$ complex cation. Coordinating atoms are shown as balls, the bispidine backbone as wireframe. Metal center, hydrogen atoms and non-coordinating residues have been omitted for clarity.

(Figure 5).[68–70] Since the energy of the triplet state of the ligand plays an important role in the sensitization of the lanthanide excited states, the photophysics of the $[GdL^2][NO_3]$ complex was examined at low temperature, in glass medium (EtOH/MeOH 4:1, 77 K) without and with a 0.1 ms delay to filter the short-lived component of emission from possible fluorescent states (Figure 6). When performing time-gated emission spectroscopy, the high energy band disappears, being then assigned to fluorescence from the relaxed singlet state ($E_{S1} = 30{,}600\ cm^{-1}$), while the long-lived well-structured band centered at ~500 nm remains, being consequently assigned to phosphorescence from the triplet state. The deconvolution of this band into 4 individual peaks allows the localization of the lowest triplet state, $E_{T1} = 22{,}500\ cm^{-1}$ (see Figures 6 and S2). This triplet excited state energy should be of sufficient energy to efficiently sensitize the main emissive states of Tb^{3+} ($^5D_4$ ~ 20,000 cm^{-1}), Eu^{3+} ($^5D_1$ ~ 19,000 cm^{-1} and $^5D_0$ ~ 17,200 cm^{-1}), and Yb^{3+} ($^2F_{5/2}$ ~ 10,000 cm^{-1}), while limiting detrimental back-energy transfer (Figure 7).[71,72]

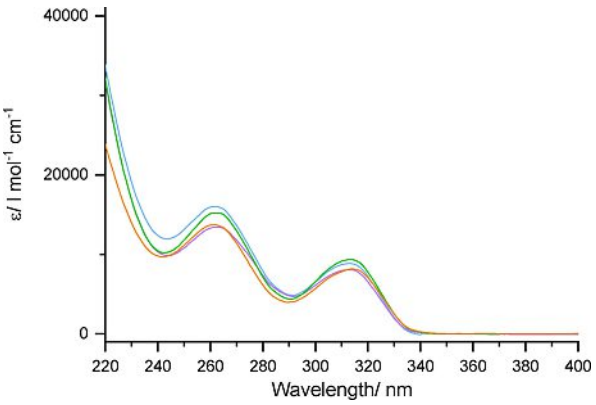

Figure 5. Molar absorptivities of 10 μM aqueous solutions of $[LnL^2][X]$ at 25 °C (Ln = Eu (orange trace), Gd (violet trace), Tb (blue trace), Yb (green trace); X = CF_3CO_2 (for Eu), NO_3).

Indeed, upon excitation of the ligand at ~315 nm, characteristic sharp emission profiles, assigned to the $^7F_J \leftarrow {}^5D_0$

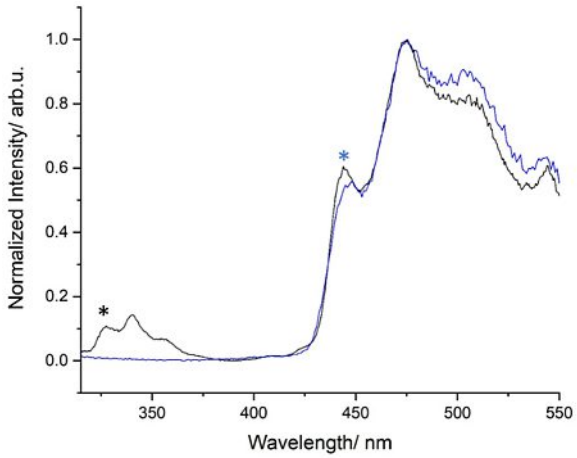

Figure 6. Emission spectra ($\lambda_{exc} = 300$ nm) of $[GdL^2][NO_3]$ without (black trace) or with (blue trace) a delay of 0.1 ms at 77 K in a mixture EtOH:MeOH (4:1). * and * represent the location of the lowest singlet and triplet state, respectively.

Table 3. Selected photophysical data of $[ML^2]^+$ in the solid and in dilute aqueous solution (H_2O, D_2O) at 298 K.

Compound	Medium	λ_{abs} [nm]	ε [$Lmol^{-1}cm^{-1}$]	λ_{em} [nm]	τ [μs]	τ_R [μs]	Φ^{Ln}_{Ln}	Φ^{L}_{Ln}	η_{sens}
$[GdL^2][NO_3]$	H_2O	262	13,500	345	–	–	–	–	–
		313	8,000						
	EtOH/MeOH – 77 K	–	–	500	–	–	–	–	–
$[EuL^2][CF_3CO_2]$	Solid State	–	–	614	1,480	3,578	0.41	0.50[a]	0.71
	H_2O (D_2O)	261	13,500	614	1,510	4,507	0.34	0.35[b]	0.97
		314	8,000		(2,150)				
$[TbL^2][NO_3]$	Solid State	–	–	544	1,200	–	–	0.71[a]	–
	H_2O (D_2O)	261	16,000	544	1,950	–	–	0.68[b]	–
		313	9,000		(2,210)				
$[YbL^2][NO_3]$	Solid State	–	–	979	5.11	–	–	–	–
	H_2O	262	15,000	979	3.54	–	–	–	–
		312	9,500						

[a] using an integrating sphere; [b] with quinine bisulfate as reference ($\Phi_f = 0.54$ in 0.5 M sulfuric acid).

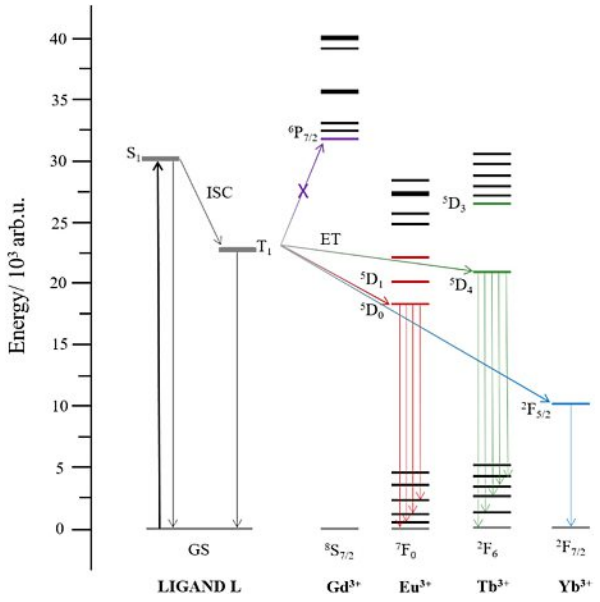

Figure 7. Jablonski Diagram for complexes $[LnL^2][X]$ (Ln = Gd, Eu, Tb, Yb; X = CF_3CO_2 (for Eu), NO_3) highlighting the possible energy transfer pathways for the efficient antenna effect.

(J = 0–4), $^7F_J \leftarrow {}^5D_4$ (J = 6–1) and $^2F_{7/2} \leftarrow {}^2F_{5/2}$ 4f–4f transitions of $[EuL^2][CF_3CO_2]$, $[TbL^2][NO_3]$ and $[YbL^2][NO_3]$, respectively, in both the solid state and diluted aqueous solution were obtained (Figure 8). In all cases, residual ligand fluorescence cannot be detected, indicating possibly an efficient sensitization process. Additionally, broad excitation spectra comparable to the absorption spectrum of the ligands were measured, confirming the antenna effect (Figures S3, S4, S8–11). The energy transfer mechanism as well as the excited states involved for each complex are compiled in Figure 7. The excited state lifetimes at the maximum wavelength were measured at room temperature for the three complexes. In every case, the decay data were fitted mono-exponentially with values of 1.48 ms, 1.20 ms and 5.11 μs, in the solid state and 1.51 ms,1.95 ms and 3.54 μs in diluted aqueous solution for the Eu^{III}, Tb^{III} and Yb^{III} complexes, respectively, suggesting the presence of one unique species in each medium. These values are significantly longer than those of the previously reported lanthanide(III) complexes with the bispidine L[1].[41] This is interpreted to be due to the incorporation of a bipyridine in the new ligand, which offers an additional donor to fully encapsulate the lanthanide center, as shown in the crystal structures. To further prove the saturation of the first coordination sphere of the lanthanide ions in solution, lifetimes were measured in natural and deuterated water (Table 3), and the hydration number q was estimated with the usual phenomenological equation.[20] The q values are 0 for both, the Eu^{III} and Tb^{III} complexes, indicating the absence of water in the first coordination sphere in solution, as expected from the ligand design and crystal structures.

The quantum yields for $[EuL^2][CF_3CO_2]$ and $[TbL^2][NO_3]$ were measured by following an absolute method in the solid state, using an integrating sphere, and by relative methods in water by using quinine bisulfate as reference (Table 3). While the values for the Eu^{III} complex are 0.50 and 0.35 for the solid state and aqueous solution, respectively, slightly higher numbers were obtained for the Tb^{III} complex, with 0.71 and 0.68, respectively. It is important to note that these values are comparable for the two media, indicating similar environments of the lanthanide complexes and minimal multiphonon deactivation by solvent relaxation. The equivalent emission spectra for solid state and solution experiments found for all three complexes, also suggest conservation of the symmetry upon solution of the complexes. The values for lifetimes and quantum yields are comparable to other well studied complexes with macrocylic ligands.[3,6,12,24,25,28]

The efficiency of the sensitization process could be further quantified in the case of the Eu^{III} complex (see Supporting Information for details), where the radiative decay was calculated from the emission spectra to be 3.58 ms and 4.51 ms in the solid state and aqueous solution respectively. These numbers result in an intrinsic quantum yield of 0.41 and 0.34, respectively, giving sensitization efficiencies of 0.71 and 0.97, respectively. While the value in the solid state is moderate, as observed for other Eu^{III} complexes,[73–74] the value in water is remarkably high, where typically enhanced quenching by the solvent is observed[73] and highlights the intense luminescent properties of these compounds in solution.

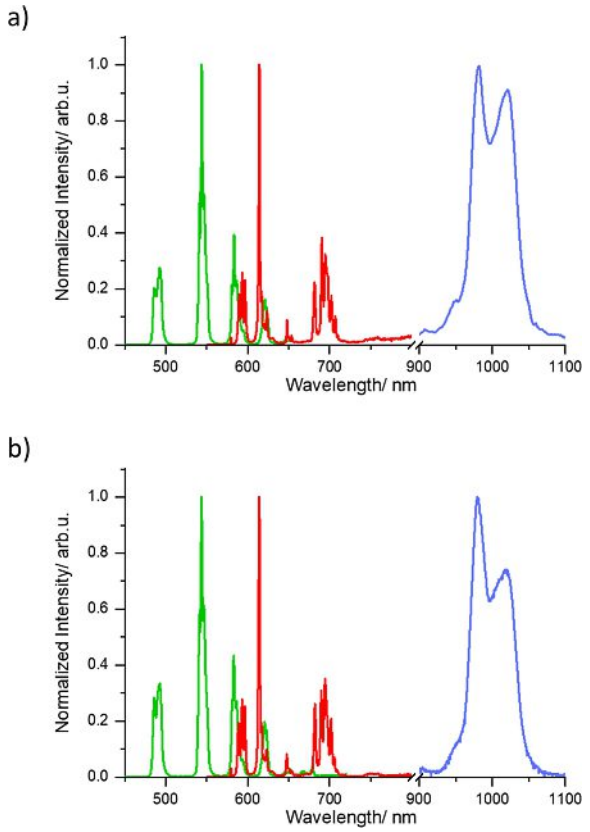

Figure 8. Emission spectra (λ_{exc} = 313 nm) of [LnL^2][NO_3] (Ln = Tb, green trace and Ln = Yb, blue trace) and [EuL^2][CF_3CO_2] (red trace) at room temperature in the solid state (a) and in diluted aqueous solution (b).

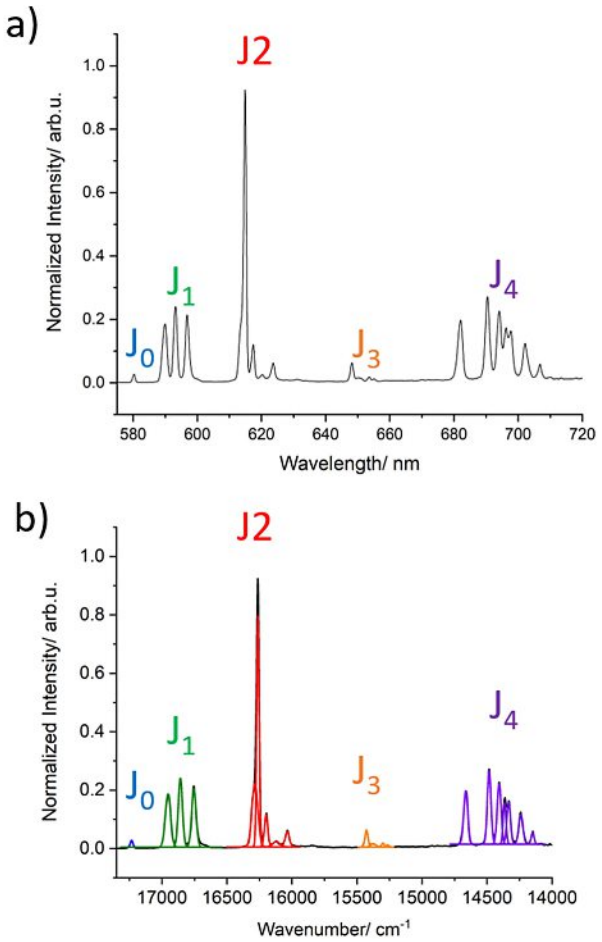

Figure 9. (a) Emission spectra (λ_{exc} = 313 nm) of [EuL^2][NO_3] in EtOH:MeOH (4:1) at 77 K. (b) Zoom of the main transition bands and their deconvolution to Gaussian curves in the wavenumber scale.

It is well-established that Eu^{III} and Yb^{III} emissions are particularly sensitive to environmental effects and in particular to variations in the first coordination sphere, making them valuable local symmetry or geometry probes.[75] Therefore, the solution structures of these complexes were studied in further detail and compared to the experimental crystal structures.[75] Experiments were performed at 77 K to reduce inhomogeneous line broadening and obtain higher resolution emission spectra (Figures 9, 10). In the case of [EuL^2][CF_3CO_2] in a mixture EtOH: MeOH (4:1) at 77 K, the observation of an intense $^7F_0 \leftarrow ^5D_0$ transition indicates that the Eu^{3+} ion occupies a site with low symmetry like C_{nv}, C_n or C_s (Figure 9). The fact that this transition, intrinsically non-degenerated (J = 0), can be fitted with a single Gaussian curve with a width at half maximum of ~20 cm^{-1}, indicates that one unique emissive species is present in solution, and therefore, no speciation occurs upon dissolution. Moreover, the $^7F_1 \leftarrow ^5D_0$ transition reflects the crystal-field splitting (CFS) of the $^7F_1$ level and additional information about the symmetry of the complex can be gained. Experimentally, we observe three clear CFS-sublevels of the $^7F_1$, present in orthorhombic or lower symmetries. In such low symmetry, the splitting of the ^7F_J transitions is expected to yield 2 J + 1 CFS-components.[76] The hypersensitive (J = 2) transition can therefore be decomposed to 5 gaussian curves, while the J = 4 transition is deconvoluted only into 7 due to overlap between the different bands (Figure 9b). Comparable features of the emission spectrum where similarly found in the solid state at low temperature, confirming the stability of the complex upon dissolution (Figures S4, S5). In addition to the crystal field splitting, the relative intensity of the $^7F_J \leftarrow ^5D_0$ transition is also a good indication of the symmetry of the complexes.[77] In this case, the emission profile in solution at 77 K presents relative intensities of 0.03, 1, 1.48, 0.11, 2.03, while values of 0.03, 1, 1.44, 0.13, 2.07 are obtained in the solid state. In both cases, the magnetic dipole transition (J = 1) was used as an internal reference. The similarity of the relative intensities confirms that the symmetry of the complex in the solid state is maintained in solution. The $^7F_4 \leftarrow ^5D_0$ transition clearly appears as the main contribution of the total emission area. In general terms, this transition is very weak for centrosymmetric compounds and becomes more intense for compounds with lower symmetry than D_{4d}, while the intensity of the J = 2 transition follows the opposite trend. Therefore, the ratio of the intensity of the J = 2 over the J = 4 transitions (R) can serve as an indicator to compare the symmetry of different complexes. In the present case, the obtained values of 0.73 and 0.70 in solution and in the solid state, respectively, indicates a rather low symmetry of the

studied complexes.[78] This value is much lower than those previously seen for TACN[22,79] or pyclen[80] based lanthanide complexes, featuring perfect C_{2v} and distorted C_3 symmetry, respectively. These features clearly indicate a low symmetrical environment of the studied complex, suggesting that the geometry can be assigned to a distorted CSAPR (C_{4v}) or a Muffin (MFF-9) polyhedron with C_s symmetry, found as the second closest geometry by shape analysis of the solid-state structure.[66]

Finally, the crystal field splitting was also studied for the Yb^{III} complex at low temperature. The line-like emission in the range of 900–1100 nm, characteristic of the $^2F_{7/2}\leftarrow{}^2F_{5/2}$ transition found at room temperature was better defined at low temperature (Figure 10). The total removal of the hot bands at ~950 nm as well as the four sublevels of the Kramers $^2F_{7/2}$ state at 10,225, 10,050, 9,900 and 9,775 cm^{-1} could clearly be distinguished. Broad total splitting of the $^2F_{7/2}$ has been previously assigned to low symmetric geometry of Yb^{3+} complexes.[81,82] In the present case, the overall splitting of the ground state $^2F_{7/2}$ is 428 and 438 cm^{-1} in solution and the solid state at 77 K, respectively, which indicates the conservation of the structure upon dissolution (Figure 10b). These values are higher than for previously reported complexes with higher D_{3h} symmetry (~350 cm^{-1})[83,84] but lower than less symmetrical examples with D_{4h} symmetry (~525 cm^{-1}),[81,85–88] pure C_2 (670 cm^{-1})[89] or really low symmetric structures (triclinic) with values over 800 cm^{-1}.[90,91] These results highly suggest that the structure of $[YbL^2][NO_3]$ is close to C_{4v} symmetry (CSAPR), in perfect agreement with the shape analysis, where it can be observed that in fact, $[YbL^2][NO_3]$ is the least CSAPR distorted of the series.

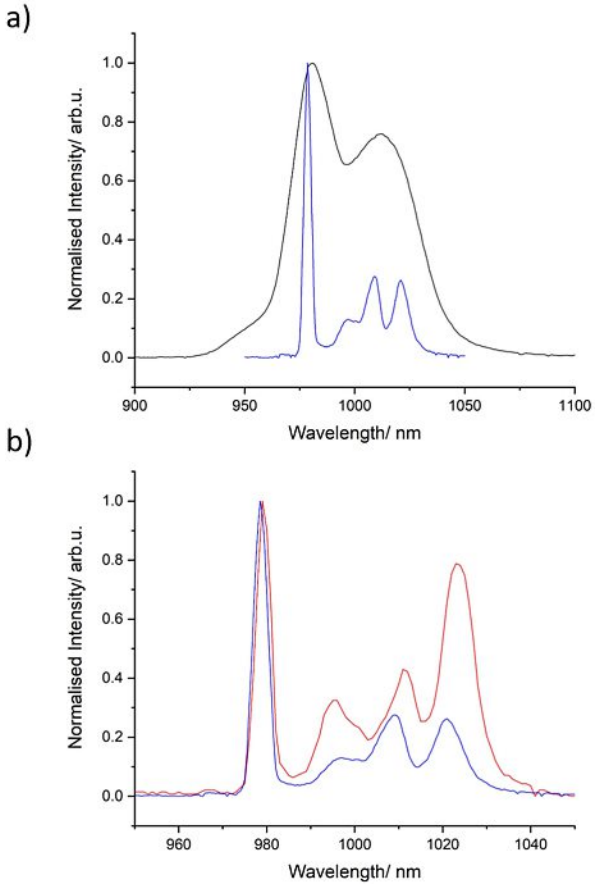

Figure 10. (a) Emission spectra (λ_{exc} = 313 nm) of $[YbL^2][NO_3]$ in aqueous solution at room temperature (black trace), in a mixture of EtOH:MeOH (4:1) at 77 K (blue trace) and (b) its low temperature emission comparison with the solid state (red trace).

Conclusion

We report the successful synthesis of the first nonadentate bispidine ligand, which leads to a fully saturated coordination sphere with Ln^{III} ions. The photophysical properties show significantly increased lifetimes compared to those with the octadentate ligand L^1 (by factors of approx. 3)[41] and exciting results in terms of quantum yields. The thorough investigation of the spectroscopic and photophysical properties allows to confirm the prediction that the structures in solution and in the solid state are identical and that solvent molecules do not coordinate directly to the metal ions. This is important information for other applications of Ln^{III} complexes of L^2 (including radiopharmaceutical probes or MRI), and it also indicates that these complexes are very stable and inert. For applications as biological fluorescence probes, red-shifted absorptions would be of interest, and modifications to achieve this goal as well as bioconjugation may be included in future work.

Supporting Information

The entire Experimental Section, the crystallographic data and information on the structural refinement, NMR and high-resolution mass spectra of all relevant ligand intermediates, ligands and complexes, as well as additional details on the photophysical experiments are given as Supporting Information.

Acknowledgements

Financial support by Heidelberg University and the German Science Foundation (Deutsche Forschungsgemeinschaft, DFG) is gratefully acknowledged. This study was conducted within the Max Planck School Matter to Life, supported by the German Federal Ministry of Education and Research (BMBF) in collaboration with the Max Planck Society. Open access funding enabled and organized by Projekt DEAL.

Conflict of Interest

The authors declare no conflict of interest.

Keywords: Lanthanides · Luminescence · Nonadentate ligand · Photophysics; Quantum Yield

[1] A. S. Chauvin, F. Gumy, D. Imbert, J. C. G. Bünzli, *Spectrosc. Lett.* **2004**, *37*, 517–532.
[2] A. de Bettencourt-Dias, P. S. Barber, S. Bauer, *J. Am. Chem. Soc.* **2012**, *134*, 6987–6994.
[3] S. Petoud, S. M. Cohen, J. C. Bunzli, K. N. Raymond, *J. Am. Chem. Soc.* **2003**, *125*, 13324–13325.
[4] E. Brunet, O. Juanes, R. Sedano, J. C. Rodriguez-Ubis, *Photochem. Photobiol. Sci.* **2002**, *1*, 613–618.
[5] M. Starck, P. Kadjane, E. Bois, B. Darbouret, A. Incamps, R. Ziessel, L. J. Charbonniere, *Chem. Eur. J.* **2011**, *17*, 9164–9179.
[6] M. Le Fur, E. Molnar, M. Beyler, O. Fougere, D. Esteban-Gomez, O. Rousseaux, R. Tripier, G. Tircso, C. Platas-Iglesias, *Inorg. Chem.* **2018**, *57*, 6932–6945.
[7] A. de Bettencourt-Dias, *Dalton Trans.* **2007**, 2229–2241.
[8] J. M. Zwier, H. Bazin, L. Lamarque, G. Mathis, *Inorg. Chem.* **2014**, *53*, 1854–1866.
[9] G. Muller, *Dalton Trans.* **2009**, 9692–9707.
[10] S. V. Eliseeva, G. Aubock, F. van Mourik, A. Cannizzo, B. Song, E. Deiters, A. S. Chauvin, M. Chergui, J. C. Bunzli, *J. Phys. Chem. B* **2010**, *114*, 2932–2937.
[11] A. D'Aléo, F. Pointillart, L. Ouahab, C. Andraud, O. Maury, *Coord. Chem. Rev.* **2012**, *256*, 1604–1620.
[12] J. W. Walton, A. Bourdolle, S. J. Butler, M. Soulie, M. Delbianco, B. K. McMahon, R. Pal, H. Puschmann, J. M. Zwier, L. Lamarque, O. Maury, C. Andraud, D. Parker, *Chem. Commun.* **2013**, *49*, 1600–1602.
[13] V. V. Rangari, S. J. Dhoble, *J. Rare Earths* **2015**, *33*, 140–147.
[14] J. Gil-Rostra, F. J. Ferrer, J. P. Espinos, A. R. Gonzalez-Elipe, F. Yubero, *ACS Appl. Mater. Interfaces* **2017**, *9*, 16313–16320.
[15] S. Shuvaev, D. Parker, *Dalton Trans.* **2019**, *48*, 4471–4473.
[16] M. Soulie, F. Latzko, E. Bourrier, V. Placide, S. J. Butler, R. Pal, J. W. Walton, P. L. Baldeck, B. Le Guennic, C. Andraud, J. M. Zwier, L. Lamarque, D. Parker, O. Maury, *Chem. Eur. J.* **2014**, *20*, 8636–8646.
[17] J. Wahsner, M. Seitz, *Inorg. Chem.* **2015**, *54*, 10841–10848.
[18] D. Kovacs, D. Phipps, A. Orthaber, K. E. Borbas, *Dalton Trans.* **2018**, *47*, 10702–10714.
[19] M. F. K. Trautnitz, C. Doffek, M. Seitz, *ChemPhysChem* **2019**, *20*, 2179–2186.
[20] A. Beeby, I. M. Clarkson, R. S. Dickins, S. Faulkner, D. Parker, L. Royle, A. S. de Sousa, J. A. G. Williams, M. Woods, *J. Chem. Soc. Perkin Trans. 2* **1999**, 493–504.
[21] R. M. Supkowski, W. D. Horrocks, *Inorg. Chim. Acta* **2002**, *340*, 44–48.
[22] A. T. Bui, M. Beyler, Y. Y. Liao, A. Grichine, A. Duperray, J. C. Mulatier, B. L. Guennic, C. Andraud, O. Maury, R. Tripier, *Inorg. Chem.* **2016**, *55*, 7020–7025.
[23] L. G. Nielsen, A. K. R. Junker, T. J. Sorensen, *Dalton Trans.* **2018**, *47*, 10360–10376.
[24] D. Kovacs, S. R. Kiraev, D. Phipps, A. Orthaber, K. E. Borbas, *Inorg. Chem.* **2020**, *59*, 106–117.
[25] J. Xu, T. M. Corneillie, E. G. Moore, G. L. Law, N. G. Butlin, K. N. Raymond, *J. Am. Chem. Soc.* **2011**, *133*, 19900–19910.
[26] A. Rodriguez-Rodriguez, D. Esteban-Gomez, A. de Blas, T. Rodriguez-Blas, M. Fekete, M. Botta, R. Tripier, C. Platas-Iglesias, *Inorg. Chem.* **2012**, *51*, 2509–2521.
[27] A. Guillou, L. M. P. Lima, D. Esteban-Gomez, N. Le Poul, M. D. Bartholoma, C. Platas-Iglesias, R. Delgado, V. Patinec, R. Tripier, *Inorg. Chem.* **2019**, *58*, 2669–2685; *Angew. Chem.* **1987**, *99*, 259–267; *Angew. Chem. Int. Ed.* **1987**, *26*, 266–267.
[28] M. Starck, J. D. Fradgley, S. Di Vita, J. A. Mosely, R. Pal, D. Parker, *Bioconjugate Chem.* **2020**, *31*, 229–240.
[29] A. Rodriguez-Rodriguez, D. Esteban-Gomez, R. Tripier, G. Tircso, Z. Garda, I. Toth, A. de Blas, T. Rodriguez-Blas, C. Platas-Iglesias, *J. Am. Chem. Soc.* **2014**, *136*, 17954–17957.
[30] A. Rodriguez-Rodriguez, M. Regueiro-Figueroa, D. Esteban-Gomez, R. Tripier, G. Tircso, F. K. Kalman, A. C. Benyei, I. Toth, A. de Blas, T. Rodriguez-Blas, C. Platas-Iglesias, *Inorg. Chem.* **2016**, *55*, 2227–2239.
[31] B. Alpha, J.-M. Lehn, G. Mathis, *Angew. Chem. Int. Ed.* **1987**, *26*, 266–267; *Angew. Chem.* **1987**, *99*, 259–261.
[32] C. Doffek, M. Seitz, *Angew. Chem. Int. Ed. Engl.* **2015**, *54*, 9719–9721; *Angew. Chem.* **2015**, *127*, 9856–9721.
[33] E. G. Moore, C. J. Jocher, J. Xu, E. J. Werner, K. N. Raymond, *Inorg. Chem.* **2007**, *46*, 5468–5470.
[34] L. J. Daumann, P. Werther, M. J. Ziegler, K. N. Raymond, *J. Inorg. Biochem.* **2016**, *162*, 263–273.
[35] L. J. Daumann, D. S. Tatum, C. M. Andolina, J. I. Pacold, A. D'Aleo, G. L. Law, J. Xu, K. N. Raymond, *Inorg. Chem.* **2016**, *55*, 114–124.
[36] E. G. Moore, A. P. Samuel, K. N. Raymond, *Acc. Chem. Res.* **2009**, *42*, 542–552.
[37] M. Shaul, Y. Cohen, *J. Org. Chem.* **1999**, *64*, 9358–9364.
[38] J. C. Bunzli, A. S. Chauvin, C. D. Vandevyver, S. Bo, S. Comby, *Ann. N. Y. Acad. Sci.* **2008**, *1130*, 97–105.
[39] E. Deiters, B. Song, A. S. Chauvin, C. D. Vandevyver, F. Gumy, J. C. Bunzli, *Chem. Eur. J.* **2009**, *15*, 885–900.
[40] P. Comba, U. Jermilova, C. Orvig, B. O. Patrick, C. F. Ramogida, K. Ruck, C. Schneider, M. Starke, *Chem. Eur. J.* **2017**, *23*, 15945–15956.
[41] F. Braun, P. Comba, L. Grimm, D.-P. Herten, B. Pokrandt, H. Wadepohl, *Inorg. Chim. Acta* **2019**, *484*, 464–468.
[42] D. G. Karraker, *J. Chem. Educ.* **1970**, *47*.
[43] J. Marçalo, A. P. De Matos, *Polyhedron* **1989**, *8*, 2431–2437.
[44] P. Comba, L. J. Daumann, R. Klingeler, C. Koo, M. J. Riley, A. E. Roberts, H. Wadepohl, J. Werner, *Chem. Eur. J.* **2018**, *24*, 5319–5330.
[45] N. Choudhary, A. Dimmling, X. Wang, L. Southcott, V. Radchenko, B. O. Patrick, P. Comba, C. Orvig, *Inorg. Chem.* **2019**, *58*, 8685–8693.
[46] N. M. Shavaleev, F. Gumy, R. Scopelliti, J. C. Bunzli, *Inorg. Chem.* **2009**, *48*, 5611–5613.
[47] A. L. Gassner, C. Duhot, J. C. G. Bünzli, A. S. Chauvin, *Inorg. Chem.* **2008**, *47*, 7802–7812.
[48] C. Piguet, J. C. G. Bünzli, G. Bernardinelli, G. Hopfgartner, A. F. Williams, *J. Am. Chem. Soc.* **1993**, *115*, 8197–8206.
[49] K. Miyata, Y. Hasegawa, Y. Kuramochi, T. Nakagawa, T. Yokoo, T. Kawai, *Eur. J. Inorg. Chem.* **2009**, *2009*, 4777–4785.
[50] P. Comba, B. Nuber, A. Ramlow, *J. Chem. Soc. Dalton Trans.* **1997**, 347–352.
[51] P. Comba, A. Lienke, *Inorg. Chem.* **2001**, *40*, 5206–5209.
[52] P. Comba, W. Schiek, *Coord. Chem. Rev.* **2003**, *238–239*, 21–29.
[53] P. Comba, M. Kerscher, W. Schiek, *Prog. Inorg. Chem.* **2007**, 613–704.
[54] P. Comba, M. Kerscher, K. Rück, M. Starke, *Dalton Trans.* **2018**, *47*, 9202–9220.
[55] I. Tomassoli, D. Gundisch, *Curr. Top. Med. Chem.* **2016**, *16*, 1314–1342.
[56] A. M. Nonat, A. Roux, M. Sy, L. J. Charbonniere, *Dalton Trans.* **2019**, *48*, 16476–16492.
[57] P. Comba, M. Kerscher, H.-J. Pietzsch, H. Spies, H. Stephan, S. Juran, in *Deutsches Patent- und Markenamt*, Germany, **2006**.
[58] P. Comba, S. Hunoldt, M. Morgen, J. Pietzsch, H. Stephan, H. Wadepohl, *Inorg. Chem.* **2013**, *52*, 8131–8143.
[59] H. Stephan, M. Walther, S. Fahnemann, P. Ceroni, J. K. Molloy, G. Bergamini, F. Heisig, C. E. Muller, W. Kraus, P. Comba, *Chem. Eur. J.* **2014**, *20*, 17011–17018.
[60] G. Singh, K. Zarschler, S. Hunoldt, I. I. S. Martinez, C. L. Ruehl, M. Matterna, R. Bergmann, D. Mathe, N. Hegedus, M. Bachmann, P. Comba, H. Stephan, *Chem. Eur. J.* **2020**, *26*, 1989–2001.
[61] C. Bleiholder, H. Börzel, P. Comba, R. Ferrari, M. Heydt, M. Kerscher, S. Kuwata, G. Laurenczy, G. A. Lawrance, A. Lienke, *Inorg. Chem.* **2005**, *44*, 8145–8155.
[62] K. Born, P. Comba, R. Ferrari, G. A. Lawrance, H. Wadepohl, *Inorg. Chem.* **2007**, *46*, 458–464.
[63] P. Barman, A. K. Vardhaman, B. Martin, S. J. Worner, C. V. Sastri, P. Comba, *Angew. Chem. Int. Ed.* **2015**, *54*, 2095; *Angew. Chem.* **2015**, *127*, 2123–2099.
[64] P. Comba, H. Rudolf, H. Wadepohl, *Dalton Trans.* **2015**, *44*, 2724–2736.
[65] M. H. Al-Sayah, R. McDonald, N. R. Branda, *Eur. J. Org. Chem.* **2004**, *2004*, 173–182.
[66] The counterion of $[EuL^2][CF_3CO_2]$ could not be identified due to the presence of numerous Fourier peaks which could be attributed to disordered water, trifluoroacetate and/or methanol. The geometry of the cation could however be established and refined satisfactorily.
[67] M. Llunell, D. Casanova, J. Cirera, P. Alemany, S. Alvare, SHAPE 2.1, Electronic Structure Group, Universitat de Barcelona, Barcelona, **2013**.
[68] L. J. Charbonniere, R. Schurhammer, S. Mameri, G. Wipff, R. F. Ziessel, *Inorg. Chem.* **2005**, *44*, 7151–7160.
[69] L. Charbonniere, R. Ziessel, M. Guardigli, A. Roda, N. Sabbatini, M. Cesario, *J. Am. Chem. Soc.* **2001**, *123*, 2436–2437.
[70] A. Nonat, C. Gateau, P. H. Fries, M. Mazzanti, *Chem. Eur. J.* **2006**, *12*, 7133–7150.
[71] F. J. Steemers, W. Verboom, D. N. Reinhoudt, E. B. van der Tol, J. W. Verhoeven, *J. Am. Chem. Soc.* **1995**, *117*, 9408–9414.

[72] M. Latva, H. Takalo, V.-M. Mukkala, C. Matachescu, J. C. Rodríguez-Ubis, J. Kankare, *J. Lumin.* **1997**, *75*, 149–169.
[73] L. Abad Galan, B. L. Reid, S. Stagni, A. N. Sobolev, B. W. Skelton, E. G. Moore, G. S. Hanan, E. Zysman-Colman, M. I. Ogden, M. Massi, *Dalton Trans.* **2018**, *47*, 7956–7964.
[74] L. Abad Galan, A. N. Sobolev, B. W. Skelton, E. Zysman-Colman, M. I. Ogden, M. Massi, *Dalton Trans.* **2018**, *47*, 12345–12352.
[75] K. Binnemans, *Coord. Chem. Rev.* **2015**, *295*, 1–45.
[76] J.-C. G. Bünzli, S. V. Eliseeva, *Lanthanide Luminescence*, Eds.: P. Hänninen, H. Härmä, Springer-Verlag, Berlin Heidelberg, **2010**, pp. 1–45.
[77] P. A. Tanner, *Chem. Soc. Rev.* **2013**, *42*, 5090–5101.
[78] H. Sund, Y. Y. Liao, C. Andraud, A. Duperray, A. Grichine, B. Le Guennic, F. Riobe, H. Takalo, O. Maury, *ChemPhysChem* **2018**, 3318–3324.
[79] A. D'Aléo, M. Allali, A. Picot, P. L. Baldeck, L. Toupet, C. Andraud, O. Maury, *C. R. Chim.* **2010**, *13*, 681–690.
[80] N. Hamon, M. Galland, M. Le Fur, A. Roux, A. Duperray, A. Grichine, C. Andraud, B. Le Guennic, M. Beyler, O. Maury, R. Tripier, *Chem. Commun.* **2018**, *54*, 6173–6176.
[81] F. Pointillart, J. Jung, R. Berraud-Pache, B. Le Guennic, V. Dorcet, S. Golhen, O. Cador, O. Maury, Y. Guyot, S. Decurtins, S. X. Liu, L. Ouahab, *Inorg. Chem.* **2015**, *54*, 5384–5397.
[82] R. F. Ziessel, G. Ulrich, L. Charbonniere, D. Imbert, R. Scopelliti, J. C. Bunzli, *Chem. Eur. J.* **2006**, *12*, 5060–5067.
[83] F. R. Gonçalves e Silva, O. L. Malta, C. Reinhard, H.-U. Güdel, C. Piguet, J. E. Moser, J.-C. G. Bünzli, *J. Phys. Chem. A* **2002**, *106*, 1670–1677.
[84] X. Yi, K. Bernot, V. Le Corre, G. Calvez, F. Pointillart, O. Cador, B. Le Guennic, J. Jung, O. Maury, V. Placide, Y. Guyot, T. Roisnel, C. Daiguebonne, O. Guillou, *Chem. Eur. J.* **2014**, *20*, 1569–1576.
[85] S. V. Eliseeva, J. C. Bunzli, *Chem. Soc. Rev.* **2010**, *39*, 189–227.
[86] E. Di Piazza, L. Norel, K. Costuas, A. Bourdolle, O. Maury, S. Rigaut, *J. Am. Chem. Soc.* **2011**, *133*, 6174–6176.
[87] G. Cosquer, F. Pointillart, J. Jung, B. Le Guennic, S. Golhen, O. Cador, Y. Guyot, A. Brenier, O. Maury, L. Ouahab, *Eur. J. Inorg. Chem.* **2014**, *2014*, 69–82.
[88] K. A. Gschneidner, J.-C. Bunzli, V. Pecharsky, *Handbook on the Physics and Chemistry of Rare Earths, Vol. 37*, 1 ed., Elsevier Science B. V., Amsterdam, **2007**.
[89] A. T. Bui, M. Beyler, A. Grichine, A. Duperray, J. C. Mulatier, Y. Guyot, C. Andraud, R. Tripier, S. Brasselet, O. Maury, *Chem. Commun.* **2017**, *53*, 6005–6008.
[90] G. Lapadula, A. Bourdolle, F. Allouche, M. P. Conley, I. del Rosal, L. Maron, W. W. Lukens, Y. Guyot, C. Andraud, S. Brasselet, C. Copéret, O. Maury, R. A. Andersen, *Chem. Mater.* **2014**, *26*, 1062–1073.
[91] G. Lapadula, D. Trummer, M. P. Conley, M. Steinmann, Y.-F. Ran, S. Brasselet, Y. Guyot, O. Maury, S. Decurtins, S.-X. Liu, C. Copéret, *Chem. Mater.* **2015**, *27*, 2033–2039.

Manuscript received: December 23, 2020
Accepted manuscript online: March 29, 2021
Version of record online: May 2, 2021

